Supporting Information

Nanocarbon Eco-Hydrogel Kit: On-Site Visual Metal Ion Sensing and Dye Cleanup, Advancing Circular Economy in Environmental Remediation

Omkar S. Nille[1], Akanksha G. Kolekar[1], Pooja V. Devre[2], Sneha V. Koparde[1], Aniket H. Sawat[1], Daewon Sohn[3], Shashikant P. Patole[4,*], Prashant V. Anbhule[1], Anil H. Gore[2,*], Govind B. Kolekar[1,*]

[1]Fluorescence Spectroscopy Research Laboratory, Department of Chemistry, Shivaji University, Kolhapur-416004, Maharashtra, India.

[2]Tarsadia Institute of Chemical Science, Uka Tarsadia University, Maliba Campus, Bardoli, Tarsadi-394350, Surat, Gujarat, India.

[3]Department of Chemistry and Research Institute for Convergence of Basic Science, Hanyang University, Seoul Campus, Seoul, South Korea.

[4]Khalifa University of Science and Technology, Abu Dhabi 127788, United Arab Emirates.

Corresponding Authors:
Prof. G. B. Kolekar
Senior Professor (Physical Chemistry), Department of Chemistry, Shivaji University, Kolhapur-416004, MS, India.
*Corresponding author: Email: gbk_chem@unishivaji.ac.in

Dr. Anil H. Gore
Assistant Professor (Analytical Chemistry),
Tarsadia Institute of Chemical Science, UKA Tarsadia University,
Bardoli-394350, Gujrat, India.
*Corresponding author: Email: anilanachem@gmail.com

Dr. Shashikant P. Patole
Associate Professor (Physics),
Khalifa University of Science and Technology, Abu Dhabi 127788, United Arab Emirates.
*Corresponding author: Email: shashikant.patole@ku.ac.ae

Materials and Methods

Text S1. Equipment

The absorption spectrum was acquired at room temperature by using Specord 210 plus, Analytikjena UV-Vis spectrophotometer with the use of 1 cm quartz cuvette. The fluorescence measurements were measured on spectrofluorometer (Model- Jasco FP 8300, Japan) equipped with xenon lamp source and 1 cm quartz cuvette. Both excitation and emission slits were fixed at 5 nm. The fluorescence lifetime (TCSPC) was measured using Horiba JobinYvon IBH DeltaFlex. High speed centrifugation was applied for purification and centrifugation of WTR-CDs (REMI R-24). The pH of solution was measured with digital pH meter model LI-120 with a combined glass electrode. The surface functional groups present in WTR-CDs, HB-Alg/Gel and HB-Alg/Gel@WTR-CDs beads were studied using a Fourier Transform Infrared Spectrometer (FTIR, Bruker Alpha, Germany). Whereas, the X-ray diffraction analysis (XRD) of WTR-CDs, HB-Alg/Gel and HB-Alg/Gel@WTR-CDs was carried out (Bruker, D8 Advance, Germany), using CuKα radiations. The particle size, morphology and elemental mapping of WTR-CDs was carried out using High resolution transmission electron microscopy (HR-TEM) (JEOL, Voltage of 300 kV) and (JEM-ARM-200F, voltage of 200 kV) (Oxford) respectively. The elemental analysis was studied using X-ray photoelectron spectroscopy (XPS) over a binding energy range of 0 to 800 eV using MgKα (1253.60 eV) as a X-Ray source (JEOL, JPS- 9030).

Text S2. Materials

The waste tea biomass was collected from the kitchen containing ingredients such as sugar, milk, tea powder and ginger (Kolhapur, India). The biopolymers and their crosslinkers were purchased from Sisco Research Laboratory (SRL), Mumbai, PVT. LTD. i.e., sodium alginate (low viscosity; 4-12 cps, G:M = 0.99, purity= 99.00 %), gelatin Powder (120 g Bloom),

calcium chloride ($CaCl_2.2H_2O$, Mol. Wt=147.02 g/mol, 99.50 %), and glutaraldehyde ($C_5H_8O_2$, Mol. Wt=100.12 g/mol, 25 %). All chemical reagents were of analytical reagent grade and used as received without further purification. The metal ions used for detection study were prepared using metal salts of $CoCl_2.6H_2O$, $CaCl_2.2H_2O$, NaCl, $ZnCl_2$, $FeCl_3.6H_2O$, $HgCl_2$, $SnCl_2.2H_2O$, $MgCl_2.6H_2O$, $FeSO_4.7H_2O$, $KMnO_4$, LiCl, $K_2Cr_2O_7$, $CuSO_4.2H_2O$, Na_2SO_3, KIO_3, KI, Na_2SO_4, $CdCl_2$, $AgNO_3$, $Cr(NO_3)_3$, $MnCl_2$, and $Pb(NO_3)_2$, etc. A stock solution (100 µg/mL) of aqueous solutions of metal ions was prepared by using respective metal salts (SRL, Mumbai, PVT. LTD.) of analytical grade with distilled water (D. W.).

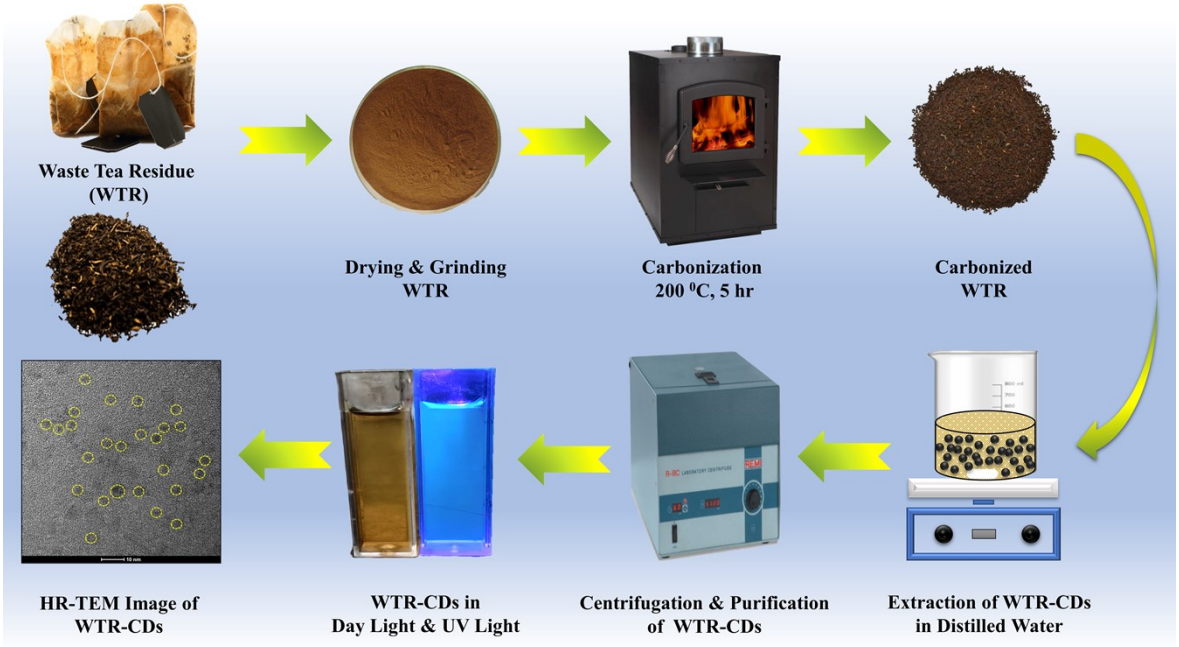

Fig S1. Schematic for the synthesis of waste tea residue carbon dots (WTR-CDs).

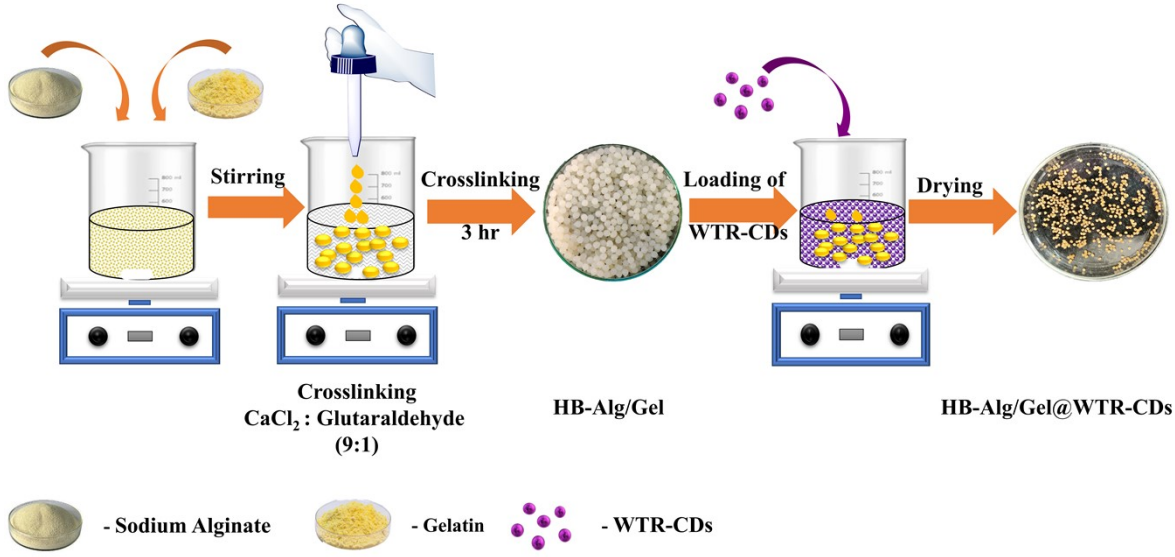

Fig S2. Schematic diagram showing preparation of HB-Alg/Gel@WTR-CDs.

Text S3. Swelling ratio study

The swelling behaviour and structural stability of materials are critical to their practical use in various applications. Swelling ratio is defined as the fractional increase in the weight of hydrogel due to water absorption.[1] The swelling ratio of beads was determined by immersing the known weighted (50 mg) dried beads in deionised water in triplicate sets. The weight of swollen beads was recorded after time interval of 0, 10, 20, 30, 40, 50, 60, 90, 120 up to 360 mins and 12 h (Figure. S6b). The excess water on surface of swollen beads was removed by tissue paper and weight of swollen beads was recorded. The swelling ratio was calculated by using below equation1.

$$\%\, Swelling = \frac{W_S - W_D}{W_D} \times 100 \qquad \text{- (1)}$$

Where, W_S = Weight of HB-Alg/Gel@WTR-CDs beads after swelling, W_D = Weight of dry HB-Alg/Gel@WTR-CDs beads.

Text S4. Quantum yield measurement

The fluorescence efficiency of WTR-CDs was quantified by measuring the quantum yield (QY). In present study, the standard comparison method was employed to calculate the QY. The well-known highly fluorescent quinine sulphate was used as a standard reference material. The aqueous solution of WTR-CDs and quinine sulphate (ϕ_{QS} = 0.54, refractive index η = 1.33) in 0.1M H_2SO_4 was used and absorbance was kept below 0.10.[2,3] The absorbance and fluorescence of respective solutions were recorded and the ϕ of WTR-CDs was calculated by using formula given below (eq. 2).

$$\Phi_{WTR-CDs} = QY = \phi_{QS} \times \left(\frac{I_{WTR-CDs}}{I_{QS}} \times \frac{A_{QS}}{A_{WTR-CDs}} \times \frac{\eta^2_{WTR-CDs}}{\eta^2_{QS}}\right) \quad \text{-(2)}$$

Where, Φ is the quantum yield, I is the integrated fluorescence intensity, whereas A is the maximum absorbance as well as η is the refractive index of QS and WTR-CDs respectively.

Results and Discussion

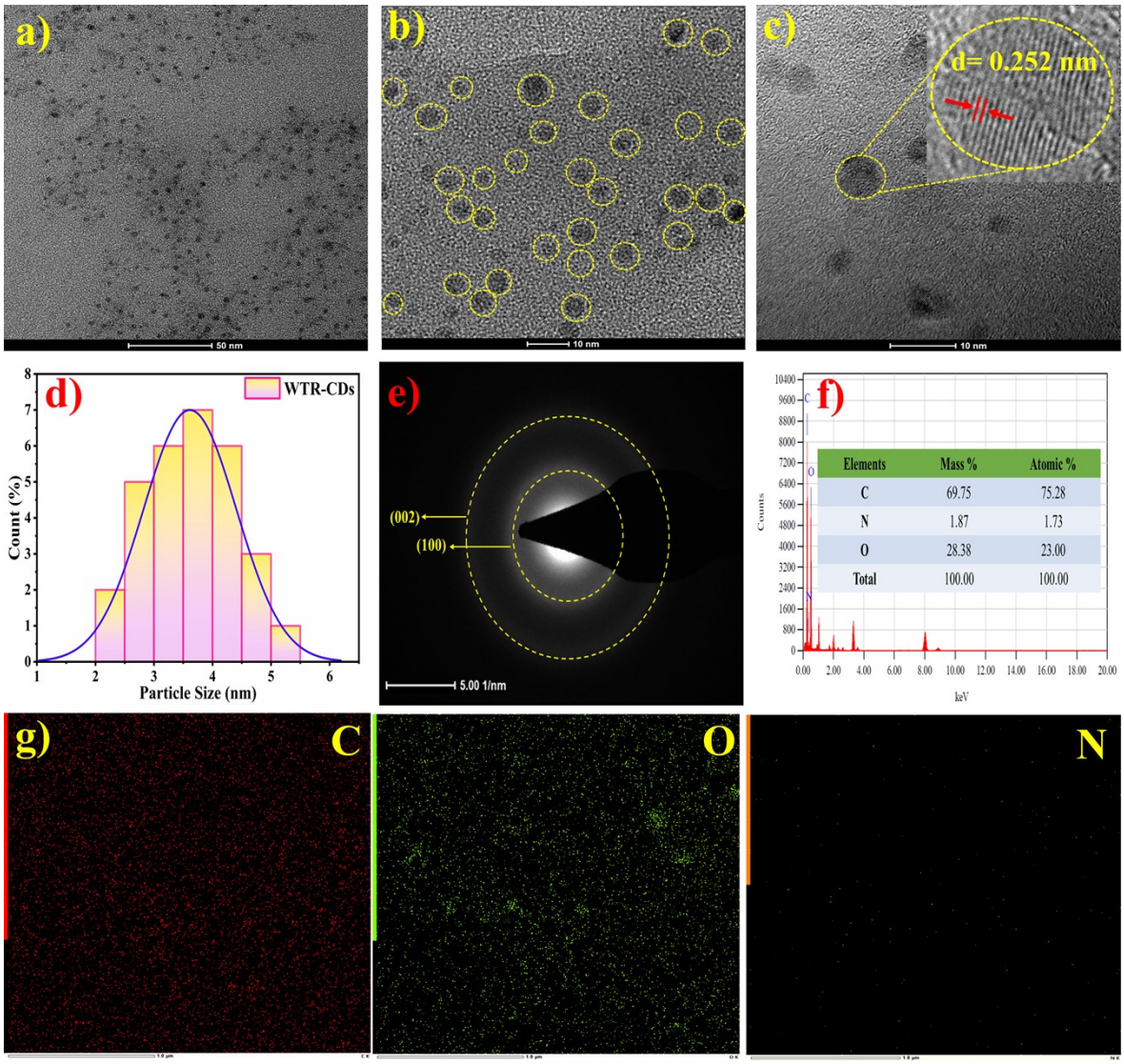

Fig S3. a-c) HR-TEM analysis, d) Particle size distribution, e) SAED pattern, f) TEM-EDX, and g) Elemental mapping of WTR-CDs.

Text S5. FTIR and XRD analysis

FTIR and XRD analysis was carried out to identify and evaluate the characteristic surface functional groups and morphological properties of WTR-CDs, HB-Alg/Gel and HB-

Alg/Gel@WTR-CDs. The Figure. S4a indicates that, the WTR-CDs mainly contains, peaks at 3342, 1639, 1093, and 1023 cm^{-1}, which confirms the presence of -OH/NH, C=C/C=O, stretching as well as bending vibrations of (C-O) of alcoholic and carboxylic functionalities, respectively. The biopolymeric HB-Alg/Gel and HB-Alg/Gel@WTR-CDs contains broad peak at 3600 to 3000 cm^{-1} is assigned to -OH/NH groups.[4] The presence of peaks at 1541 cm^{-1} and 1242 cm^{-1} belongs to stretching vibrations of C-N, and N-H (amide) functionalities belongs to gelatin.[5] In addition, the -C-H stretching vibrations of the polymeric methyl ($-CH_3$) and methylene ($-CH_2$) groups are assigned at 2924 cm^{-1} and 2857 cm^{-1}, respectively. The symmetric and asymmetric stretching vibrations of at 1639 cm^{-1} and 1384 cm^{-1} belongs to $-COO^-$ functionality, which electrostatically interacts with the functional groups of WTR-CDs. Further, the C-O and C-C stretching signals were observed at 1093 cm^{-1} and 1023 cm^{-1}. The small peak at 469 cm^{-1} indicates that presence of Ca^{2+} used as a crosslinker.

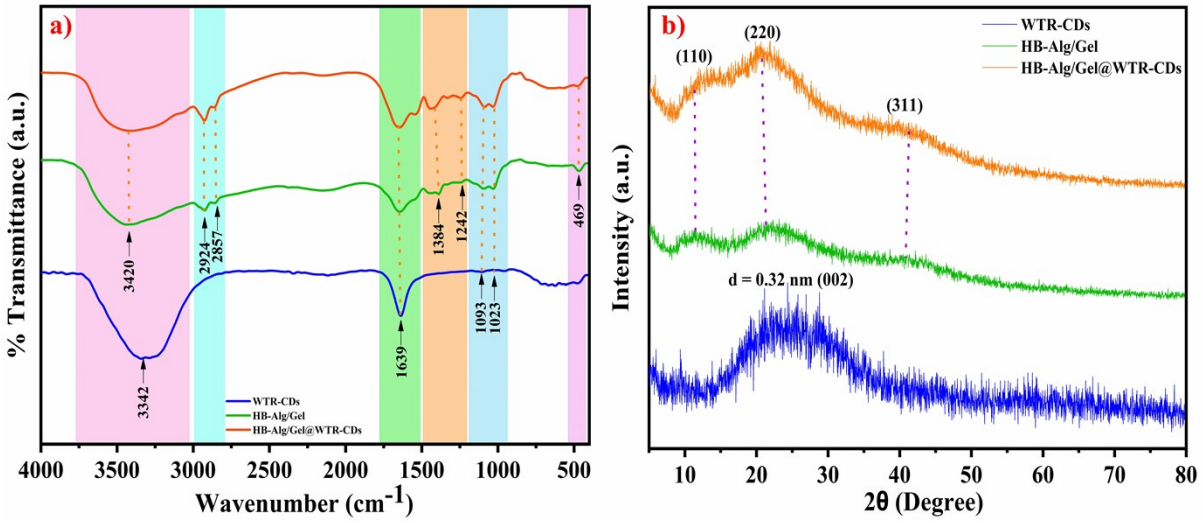

Fig S4. a) FTIR and, b) XRD spectra of (i) WTR-CDs, (ii) HB-Alg/Gel and, (iii) HB-Alg/Gel@WTR-CDs.

The X-ray diffraction analysis (XRD) was used as a prominent tool to understand the morphological, structural properties and crystallinity of WTR-CDs, HB-Alg/Gel as well as HB-Alg/Gel@WTR-CDs. In Figure. S4b, the WTR-CDs shown broad peak at 23.60º with

(002) hkl planes having d = 0.32 nm interplanar spacing. All the materials having a broad peak at around ~20º confirming the amorphous nature which correlated with distance between amino acid residues.[4] Further, three characteristic peaks profound at 2θ values 11.48º (110), 20.85º (220), and 40.39º (311) well matched with the peaks of alginate having α-1-guluronic acid as well as β-D-mannuronic acid.[6–8] Also, the broad peak in the 2θ range from 10º-30º, well defines the amorphous nature of gelatin into polymer matrix.[4,5] The non-intense peaks present in the prepared HB-Alg/Gel and HB-Alg/Gel@WTR-CDs were due to the electrostatic and hydrogen bonding interactions between surface functional groups of polymers and WTR-CDs.[1] The change in the XRD peak pattern of pristine and nanocomposite hydrogels confirms the formation of nanocomposite HB-Alg/Gel@WTR-CDs.

Text S6. FE-SEM and EDX analysis

The interior morphology of pristine HB-Alg/Gel and HB-Alg/Gel@WTR-CDs was observed using FE-SEM and EDX analysis and demonstrated in Figure. S5 a-d. The pristine HB-Alg/Gel showing porous morphology with irregular internal hydrogel network (Figure. S5a). Whereas, in case of HB-Alg/Gel@WTR-CDs the drastic changes were noticed as the CDs are incorporated into hydrogel matrix. The observable reduction in pores of hydrogel network with incorporation of CDs proving the formation of crosslinking and interaction of WTR-CDs with functional groups of polymer network (Figure. S5c). The EDX analysis of both pristine and CDs loaded hydrogel systems indicating dramatic change in carbon percentage confirming the successful loading of CDs into hydrogel matrix. As shown in Figure. S5b and S5d, the percentage of carbon is increased from 41.43 to 53.32 wt% in case of HB-Alg/Gel and HB-Alg/Gel@WTR-CDs respectively. The significant change in morphology of pristine and CDs loaded hydrogels signifies that, WTR-CDs are effectively crosslinked with polymer matrix.

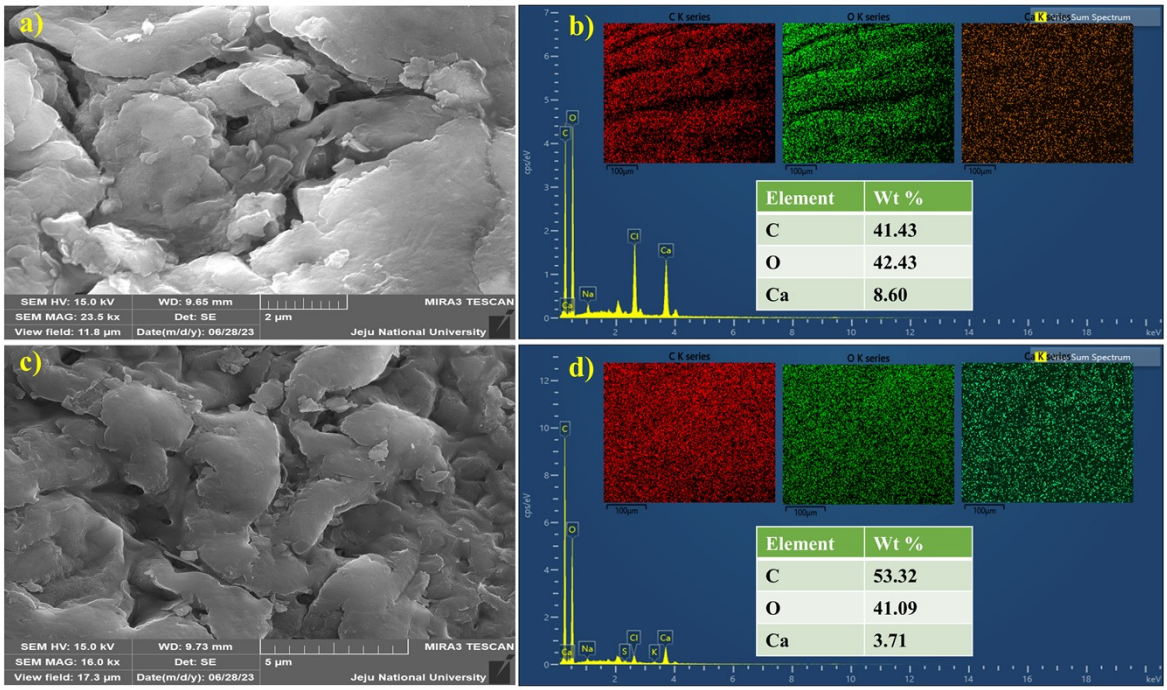

Fig S5. The morphology and EDX of a, b) HB-Alg/Gel, and c, d) HB-Alg/Gel@WTR-CDs.

Text S7. pH Effect

The stability of the material is one of the important parameters as per the practical applicability concerned. The fluorescence stability of WTR-CDs was investigated at various pH ranges i.e., acidic to basic (2-12 pH). The study was carried out in triplicate (n= 3) to investigate the reproducibility as well as stability of the WTR-CDs. In present study, the Figure. S6a reveals that, the WTR-CDs were interacted with broad range of pH, and fluorescence was recorded (λ_{ex}= 380 nm). The obtained results indicated that, the WTR-CDs showed maximum fluorescence intensity at each pH monitored. The synthesized WTR-CDs shown almost stable fluorescence intensity at studied pH range, proving that the CDs can be effectively applicable at every pH range.

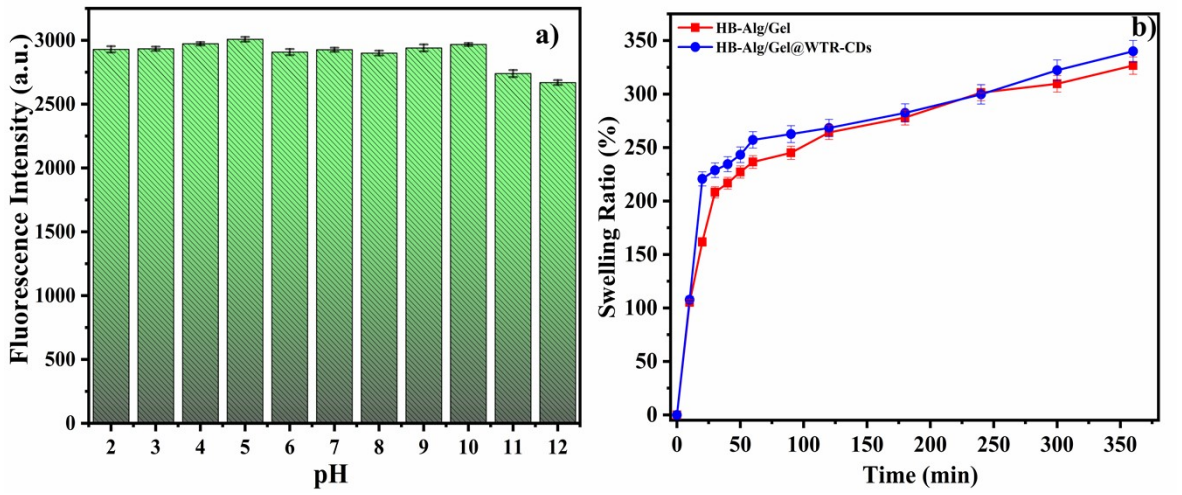

Fig S6. a) The effect of pH (2-12) on fluorescence intensity of WTR-CDs, and b) swelling behavior of HB-Alg/Gel and HB-Alg/Gel@WTR-CDs hydrogel beads. (pH = 2-12, V= 10 mL, $W_{HB\text{-}Alg/Gel@WTR\text{-}CDs}$ = 50 mg) (n= 3).

Text S8. Swelling Study

The swelling efficiency of HB-Alg/Gel beads and HB-Alg/Gel@WTR-CDs was found to be 105.26±2.63% and 107.66±3.23% within 10 minutes respectively (Figure. S6b). The swelling efficiency suddenly increases up to 161.80±4.04 % and 220.73±6.62 % within 20 minutes, respectively. Then the swelling of HB-Alg/Gel and HB-Alg/Gel@WTR-CDs gradually increases up to 309.66±7.74 % and 322.33±9.67 % respectively. The maximum swelling of both HB-Alg/Gel and HB-Alg/Gel@WTR-CDs in 360 mins was found to be 326.66±8.16 % and 340.00±10.20 % respectively. From the swelling study we can clearly found that, the HB-Alg/Gel and HB-Alg/Gel@WTR-CDs hydrogel beads are highly and rapidly swelling in nature.

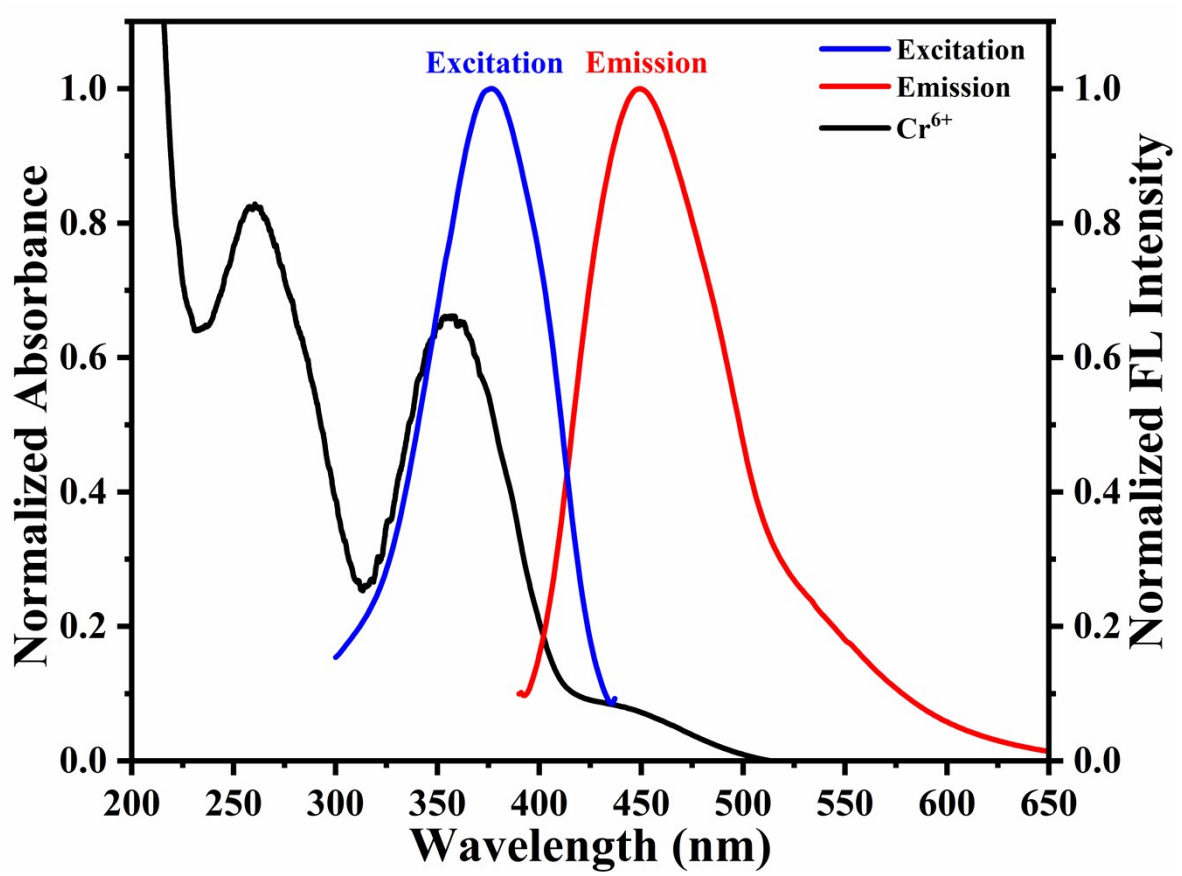

Fig S7. The excitation and emission spectra of HB-Alg/Gel@WTR-CDs and absorbance spectra of Cr^{6+}.

Table No. S1: The comparison of different CDs based hydrogels for chromium and manganese ion determination.

Sr. No.	Fluorescent Probe	Polymers used for preparation of Hydrogel	Polymer Composite Hydrogel	Analyte	Linear Range for Detection	Limit of Detection (LOD)	Reference
1	Carbon dots from chitosan hydrogel (CD)	Agarose	Agr/CD hydrogel film	Cr^{6+}, Cu^{2+}, Fe^{3+}, Pb^{2+}, Mn^{2+}	1 pM – 1 mM	Cr^{6+} = 1.00 pM, Cu^{2+} = 0.50 µM, Fe^{3+} = 0.50 nM, Pb^{2+} = 0.50 nM, Mn^{2+} = 0.50 nM	9
2	QCDs from 2-amino-2-methyl-1-propanol	Polyvinylpyrrolidone (PVP)	ZnO-QCD-hydrogel	Cr^{6+}	0-1.25 mM	1.20 µM	3
3	Rice fried codonopsis pilosula (CP) derived carbon dots (CP-CDs)	Agarose	CD-CDs hydrogel sheet	Cr^{6+}	0.03 to 50.00 µM	15.00 nM	10
4	Syzygium cumini fruits derived carbon dots (CDs)	Agarose	GSH-capped CD-agarose hydrogel film	Pb^{2+}, Fe^{3+}, Mn^{2+}	0.005 to 0.075 mM, 0.0075 to 0.10 mM, 0.0075 to 0.10 mM	Pb^{2+} = 1.30 µM, Fe^{3+} = 2.50 µM, Mn^{2+} = 2.10 µM	11
5	Nitrogen doped carbon dots (NCDs)	Agar powder	NCDs@hydrogel strip	MnO_4^-, Au^{3+}	510 nM – 2 µM, 3.89 – 20 µM	MnO_4^- = 170.00 nM, Au^{3+} = 1.28 µM	12
6	Citric acid and ethylenediamine derived CD	Chitosan, cellulose nanocrystals	CS/CNCD composite hydrogel	Cr^{6+}	0.10-1.00 µg/L	0.04 µg/L	13
7	Citric acid and ethylenediamine based amino modified CDs	Cellulose nanofibers (CM-CNF)	(CM-CNF-CDs)	Cr^{6+}	10-50 mg/L	4.20 mg/L	14
8	Citric acid and ethylenediamine derived	Cellulose nanocrystals (CN),	CS/CNCD composite hydrogel	Cr^{6+}	0.10 –1.00 µg/L	0.04 µg/L	13

	CDs	Chitosan (CS)					
9	Citric acid and ethylenediamine derived CDs	Chitosan, Cellulose nanofires	Fluorescent magnetic chitosan-based hydrogel (FMCH)	Cr^{6+}	20-800 mg/L	14.20 mg/L	[15]
10	**Waste tea residue carbon dots (WTR-CDs)**	**Sodium Alginate, Gelatin**	**HB-Alg/Gel@WTR-CDs**	**Cr^{6+}, Mn^{7+}**	**0 – 10 µg/mL**	**Cr^{6+} = 0.28 µg/mL, Mn^{7+} = 0.30 µg/mL**	**Present Work**

References:

1 S. Saber-Samandari, S. Saber-Samandari, H. Joneidi-Yekta and M. Mohseni, *Chem. Eng. J.*, 2017, **308**, 1133–1144.

2 D. B. Gunjal, Y. M. Gurav, A. H. Gore, V. M. Naik, R. D. Waghmare, C. S. Patil, D. Sohn, P. V. Anbhule, R. V. Shejwal and G. B. Kolekar, *Opt. Mater. (Amst).*, , DOI:10.1016/j.optmat.2019.109484.

3 A. Truskewycz, S. A. Beker, A. S. Ball, B. Murdoch and I. Cole, *Anal. Chim. Acta*, 2020, **1099**, 126–135.

4 J. S. Marciano, R. R. Ferreira, A. G. de Souza, R. F. S. Barbosa, A. J. de Moura Junior and D. S. Rosa, *Int. J. Biol. Macromol.*, 2021, **181**, 112–124.

5 P. Sirajudheen, P. Karthikeyan, K. Ramkumar and S. Meenakshi, *Int. J. Biol. Macromol.*, 2020, **164**, 3055–3064.

6 A. Shameem, P. Devendran, V. Siva, K. S. Venkatesh, A. Manikandan, S. A. Bahadur and N. Nallamuthu, *J. Inorg. Organomet. Polym. Mater.*, 2018, **28**, 671–678.

7 P. V. Devre, A. S. Patil, D. Sohn and A. H. Gore, *J. Environ. Chem. Eng.*, 2023, **11**, 109368.

8 T. Zaineb, B. Uzair, W. Y. Rizg, W. S. Alharbi, H. M. Alkhalidi, K. M. Hosny, B. A. Khan, A. Bano, M. Alissa and N. Jamil, *Pharmaceutics*, , DOI:10.3390/pharmaceutics14122764.

9 N. Gogoi, M. Barooah, G. Majumdar and D. Chowdhury, *ACS Appl. Mater. Interfaces*, 2015, **7**, 3058−3067.

10 Y. Qiu, D. Gao, H. Yin, K. Zhang, J. Zeng, L. Wang, L. Xia, K. Zhou, Z. Xia and Q. Fu, *Sensors Actuators, B Chem.*, 2020, **324**, 128722.

11 J. R. Bhamore, T. J. Park and S. K. Kailasa, *J. Anal. Sci. Technol.*, , DOI:10.1186/s40543-020-00208-8.

12 V. M. Naik, D. B. Gunjal, A. H. Gore, P. V. Anbhule, D. Sohn, S. V. Bhosale and G. B.

Kolekar, *Anal. Bioanal. Chem.*, 2020, **412**, 2993–3003.

13 H. Zeng, Z. Hu, C. Peng, L. Deng and S. Liu, .

14 Q. Luo, H. Yuan, M. Zhang, P. Jiang, M. Liu, D. Xu, X. Guo and Y. Wu, *J. Hazard. Mater.*, 2021, **401**, 123432.

15 Y. Luo, Z. Hu, X. Lei, Y. Wang and X. Guo, *Colloids Surfaces A Physicochem. Eng. Asp.*, 2023, **658**, 130673.